JMEPEG (1992) 1: 695-704

Specimen Edge Effects on Bending Fatigue of Carburized Steel

R.E. Cohen, D.K. Matlock, and G. Krauss

The effects of specimen geometry on the fatigue behavior of SAE 4320 steel carburized at 927 °C were evaluated with two sets of cantilever bend specimens, one set machined with square edges and one set machined with round edges. The specimens with square edges exhibited a 13% lower fatigue limit. In comparison to the rounded samples, the lower fatigue limit in the square-edged samples was attributed to the presence of a higher volume fraction of retained austenite in the sample corners and a lower surface residual compressive stress. As a result of the differences in residual stress, preferential crack initiation sites existed in the square-edged samples at a location approximately 200 to 900 μm from the square edge. The implications of this study on laboratory analyses of the bending fatigue performance of carburized gear steels are discussed.

1. Introduction

A recent review of the bending fatigue performance of carburized steel identified a wide range of reported fatigue limits.[1] The variations in fatigue behavior may not only reflect differences in processing history and microstructure, but also differences in specimen geometry. Coarse carbide particles and excessive retained austenite at the square edges of carburized cantilever bend specimens have been shown to serve as preferred sites for fatigue crack initiation.[2,3] This information was developed in a study of SAE 8620 and EX24 steels vacuum carburized at 1050 °C (1920 °F). The high carbon level introduced into austenite at 1050 °C could not be effectively lowered at the square specimen edges during the diffusion portion of the carburizing cycle. As a result, undesirable microstructures developed and served as fatigue crack initiation sites, thus reducing bending fatigue performance.

To provide a better assessment of the effects of alloying, processing, and microstructure on fatigue of carburized steel, several studies subsequent to that of Jones and Krauss[2,3] have used cantilever bend specimens with rounded edges.[4,5] The rounded edges develop a uniform case depth after carburizing and eliminate at least one cause of the variations observed in measuring bending fatigue performance.

Another approach to avoiding undesirable corner microstructures has been to copper plate square-edged bending fatigue specimens before final grinding of the tension surface.[6] The copper plating on the side surfaces prevents excessive carbon concentration at corners, resulting in a uniform case along the line of maximum stress.

Although Jones and Krauss[2,3] reported the undesirable microstructures developed in square-edged specimens, their work was not designed to examine specimen geometry effects, and no comparison with round-edged specimens was performed. The subsequent work of Erven and Pacheco[4,5] investigated alloying and processing influences on bending fatigue performance with round-edged specimens to eliminate the detrimental corner effect, but no direct comparison was made between square and round-edged specimens. In addition, carburizing at a lower temperature than used by Jones and Krauss, around 930 °C (1700 °F), a temperature typically used for gas carburizing, may reduce the potential carbon saturation of austenite during the initial boost stage of carburizing and, therefore, may not cause the excessive carbon retention noted by Jones and Krauss.

The purpose of the present study is to measure the influence of specimen geometry on the bending fatigue of carburized steel, with a comparison of two sets of SAE 4320 steel specimens. Both sets of specimens, one with square edges and one with round edges, were identically carburized at the same time at 927 °C (1700 °F). The information developed in this study provides an estimate of the extent to which specimen geometry affects microstructure and fatigue of conventionally carburized steel. This influence of geometry may be useful for the evaluation of specimen designs for the study of bending fatigue in case-hardened steel and may serve as a guide when interpreting results, given the wide range of reported bending fatigue limits.

Specimen geometry has been recognized as an influence on bending fatigue performance. Three-point bend, four-point bend, cantilever beam, and rotating beam specimens have been used to evaluate fatigue of carburized steel. Variations in specimen geometry exist because of differences in starting material, machining capability, and testing machine configuration and capacity. The next section briefly reviews the various types of cantilever specimens that have been used to evaluate bending fatigue of carburized steel.

2. Specimen Design

Figure 1 summarizes various cantilever bend specimens that have been used to evaluate fracture and fatigue of carburized steels over the past 35 years.[7-13] The Brugger design, shown in Fig. 1(a), was developed to evaluate toughness and fatigue of carburized steel. The Brugger specimen design was altered by other investigators to accommodate machining considerations and fatigue testing machine capability. DePaul[9] defines three requirements for Brugger-type cantilever bend specimens: (1) an abrupt change in cross section to act as a

R.E. Cohen, D.K. Matlock, and **G. Krauss,** Advanced Steel Processing and Products Research Center, Colorado School of Mines, Golden, Colorado.

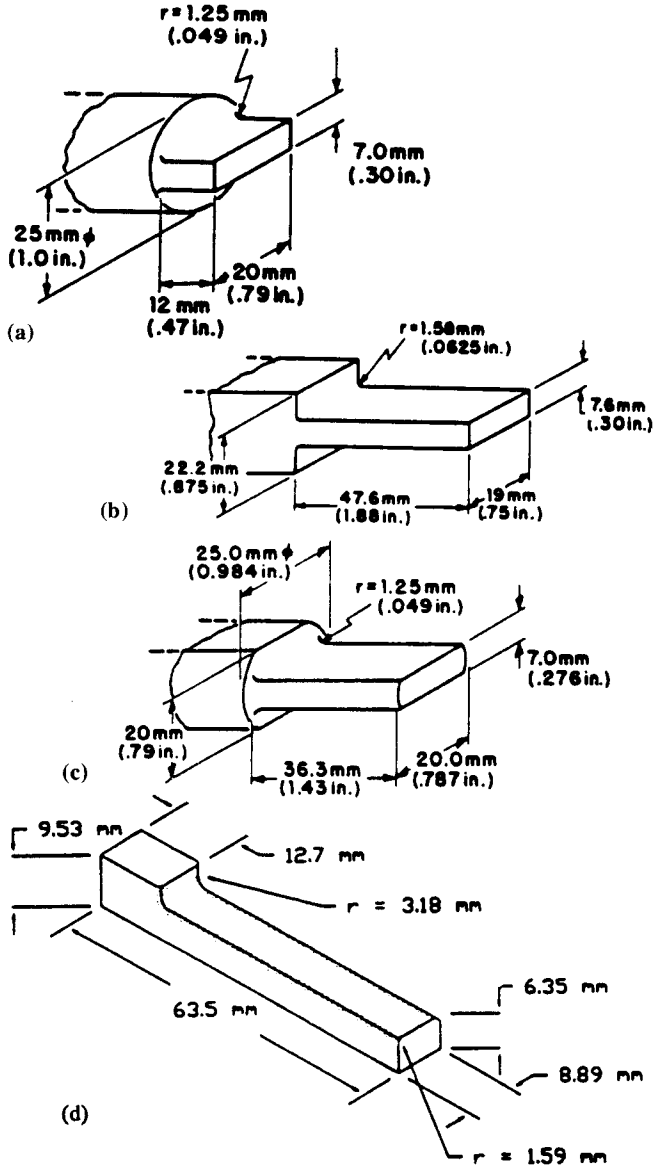

Fig. 1 Cantilever bend specimens used to evaluate fatigue and fracture of carburized steel. **(a)** Brugger design.[7] **(b)** DePaul.[9] **(c)** Diesburg.[8,12] **(d)** Jones, Pacheco, Erven[2-5,13] **(a), (b),** and **(c)** from Ref 8.

stress raiser, (2) provision for external bending load application, and (3) an adequate width-to-thickness ratio to provide a multiaxial stress state within the specimen. To satisfy these criteria, DePaul used the test specimens shown in Fig. 1(b), a geometry which produced stress distributions similar to gear segments under equivalent loading conditions.[9]

The DePaul specimen was used for both impact and high-cycle fatigue investigations.[9-11] Figure 1(c) shows a composite of the Brugger and the DePaul designs, which Diesburg and his colleagues used for impact, low-cycle impact fatigue, high-cycle bending fatigue, and combined loading testing.[8,12]

Jones, Pacheco, and Erven studied bending fatigue of carburized steel with the specimen design in Fig. 1(d).[2-5,13] In comparison to the original Brugger specimen in Fig. 1(a), the root radius at the section change was increased to 3.18 mm, the specimen width was reduced to 8.89 mm, and the beam length was extended to 63.5 mm. This design provides economical specimens that accommodate readily available, modest capacity, testing machines.

Table 1 Characteristics of Various Bending Fatigue Specimens

Ref	Radius, mm	Width/thickness	K_t	Comments
Brugger and Kraus 1961[7]	1.25	2.9	1.6	Square edges
DePaul 1970[9] deBarbadillo 1973[11]	1.58	2.5	1.5	Square edges
Diesburg and Eldis 1978[12]	1.25	2.9	1.6	Square edges
Jones and Kraus 1978[2,3]	3.18	1.4	1.3	Square edges
Pacheco and Kraus 1988[5]	3.18	1.4	1.3	Rounded edges
Erven 1990[4,13]	3.18	1.4	1.3	Rounded edges

Note: K_t from Ref 15.

In cantilever beam fatigue testing, the applied stress is calculated using simple beam equations assuming elastic behavior and uniform stress across the specimen. The stress can also be calculated from strain gage measurements obtained at the base of the radius, again assuming uniform stress across the specimen.

Table 1 lists the critical dimensional parameters of section change radius and width/thickness ratio, and the stress concentration, K_t, at the section change for the four specimen designs. The design used by Jones, Pacheco, and Erven has a larger radius, resulting in a lower K_t than previous specimen designs. The width/thickness ratio is also lower, although the effect of width/thickness ratio is generally not significant in the range of stresses used in bending fatigue testing of carburized steel.

As noted earlier, the edges of the specimens were rounded after Jones and Krauss measured carbon buildup and resultant undesirable microstructure at the square edges of the specimens.[2,3] In addition to the direct measurement of Jones and Krauss, finite-element modeling of the carbon diffusion process predicts excess carbon at square corners.[14] Rounding the specimen edges allows uniform carbon diffusion, avoiding confounding edge effects that increase the scatter in fatigue data.[5,13]

The stress concentration effect of the radius was illustrated by two-dimensional finite-element modeling (FEM) of a vertical plane through the center of the specimen shown in Fig. 1(d). Figure 2 shows the results from the finite-element model for a given displacement.[13] The arrow in Fig. 2 indicates the point of maximum stress in the two-dimensional cross section. The location of the point of maximum stress was in excellent agreement with strain gage measurements, showing the line of maximum stress to be along the base of the radius of the specimen.[13]

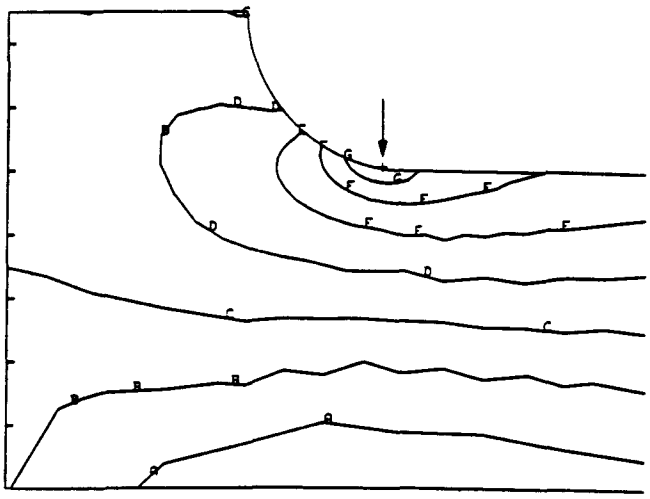

Fig. 2 Stress contours in the area of the specimen radius generated by finite-element modeling. The arrow indicates the point of maximum stress.

Table 2 Chemical Composition of SAE 4320 Bar

Composition, wt%										
C	Mn	P	S	Si	Cr	Ni	Mo	Cu	Al	Ti
0.2	0.61	0.012	0.018	0.25	0.56	1.77	0.26	0.19	0.03	0.003

Table 3 Carburizing Process

Description	Time, min	Temperature °C	Temperature °F	Atmosphere carbon potential, %
Heat.....	18	921	1690	0
Carburize....	135	927	1700	1.05
Diffuse.....	135	927	1700	0.82
Equalize.....	30	849	1560	0.82

3. Experimental Procedures

Modified Brugger specimens were machined from 15-cm (6-in.) diameter SAE 4320 bar with the long axis of the specimen oriented perpendicular to the bar rolling direction, as shown in Fig. 3. Table 2 lists the chemical composition of the heat studied. Two sets of samples were machined, one with round edges and one with square edges with the geometries shown in Fig. 4.

The bending fatigue specimens were sanded through 320-grit polishing paper and chemically polished in a HF-H_2O_2-H_2O solution. All specimens were carburized as shown in Table 3, oil quenched at 65 °C (150 °F) and tempered at 150 °C (300 °F) for 1 hr.

After carburizing, surface roughness measurements, R_a, were obtained on all specimens at the base of the radius, along the line of maximum stress. Surface residual stress X-ray measurements were taken near the edges and at the center of the line of maximum stress for both specimen geometries.[16]

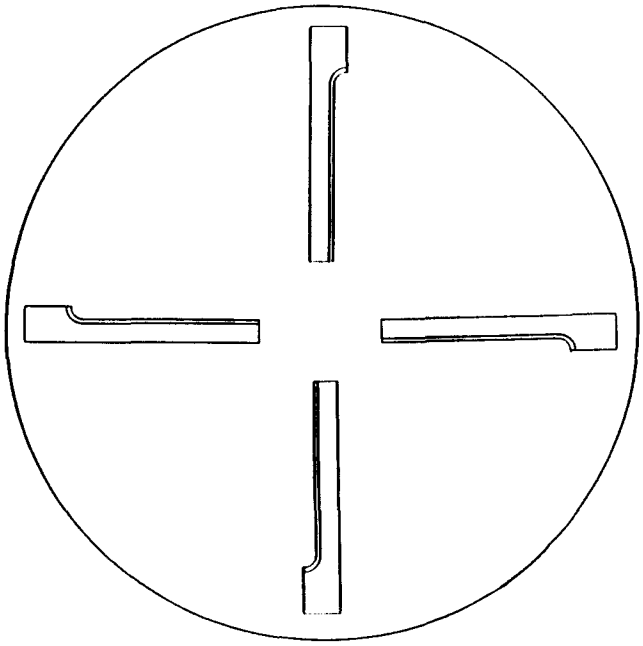

Fig. 3 Orientation of specimens machined from 15-cm diam SAE 4320 bar.

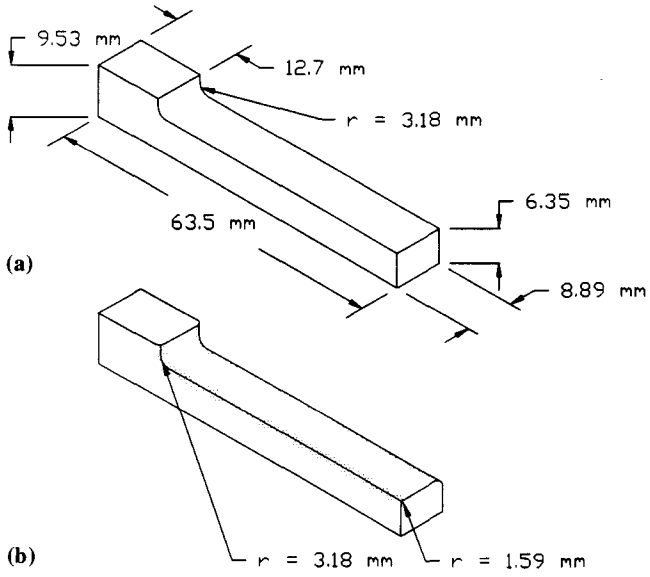

Fig. 4 Fatigue specimen geometries. **(a)** Square edges. **(b)** Same dimensions as **(a)**, but with rounded edges.

The specimens were tested in cantilever bending fatigue in the as-heat treated condition with a displacement-controlled machine operating at 30 Hz. The minimum/maximum load ratio was 0.1, and 2×10^6 cycles without failure was used as the run-out criterion. The applied stresses were calculated with

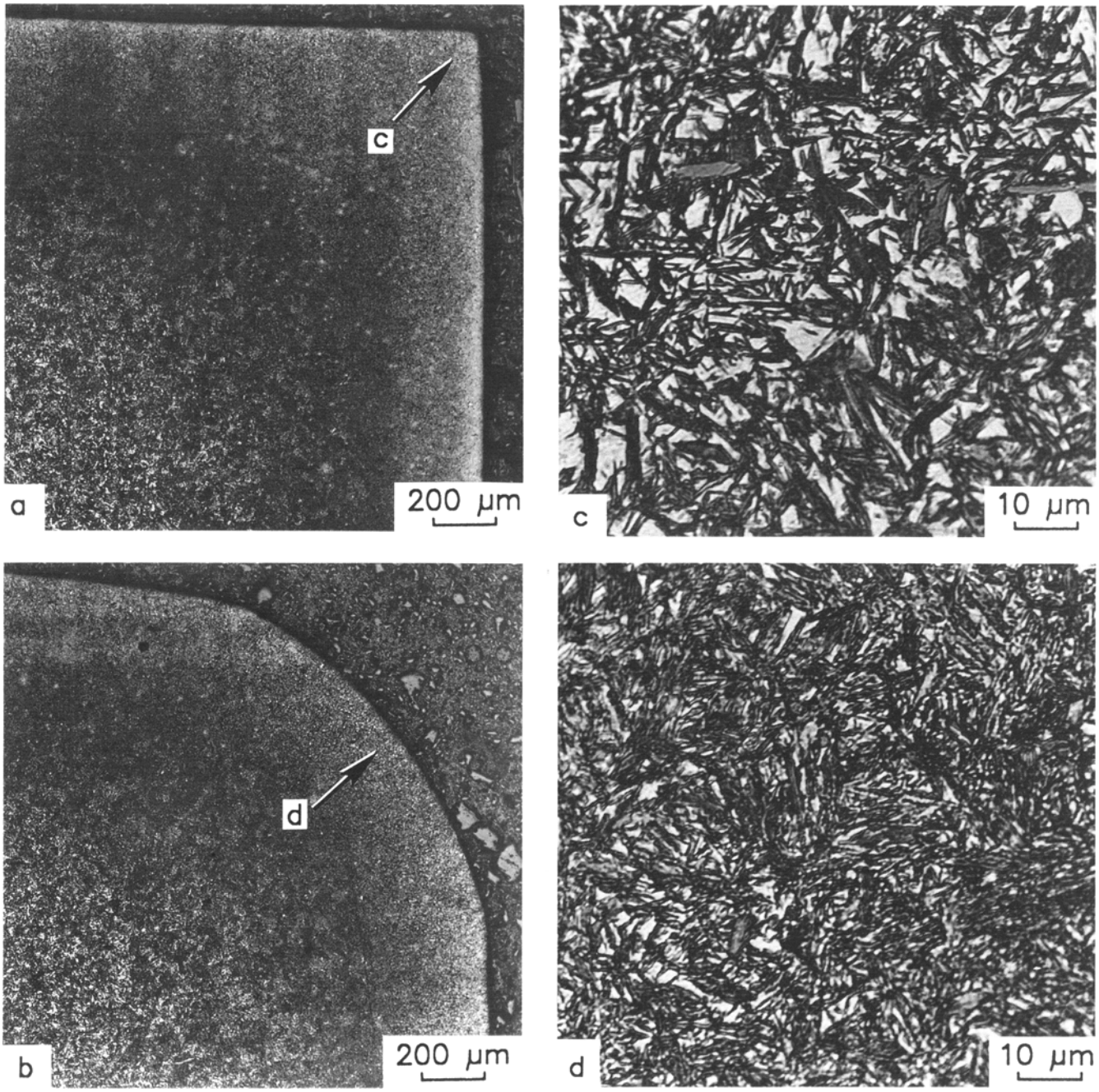

Fig. 5 Microstructures of SAE 4320 bending fatigue specimens. (**a**) and (**b**) Low magnification showing case and core of each geometry. (**c**) and (**d**) Case microstructures near square and round edges, respectively. Light micrographs, 2% nital etch.

beam equations including the full width of the specimens, giving a conservative value for the round-edged geometry. Stress levels were confirmed with strain-gaged specimens.

Case and core microstructures were revealed by a 2% nital etch on mounted and polished specimen cross sections. Prior austenite grain boundaries were observed after etching in a solution containing 500 ml of saturated picric solution in distilled water and 5 g of sodium tridecylbenzene as a wetting agent.[17] Ten drops of hydrochloric acid were added per 100 ml of the above stock solution. Included in the microstructural examination were measurements of prior austenite ASTM grain size, depth of surface intergranular oxidation, and microhardness profiles. Fracture surfaces were characterized by examination with a scanning electron microscope (SEM).

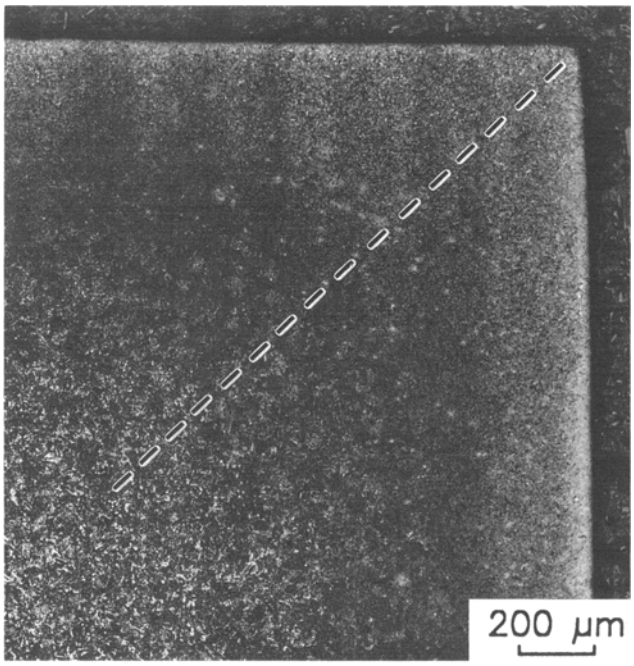

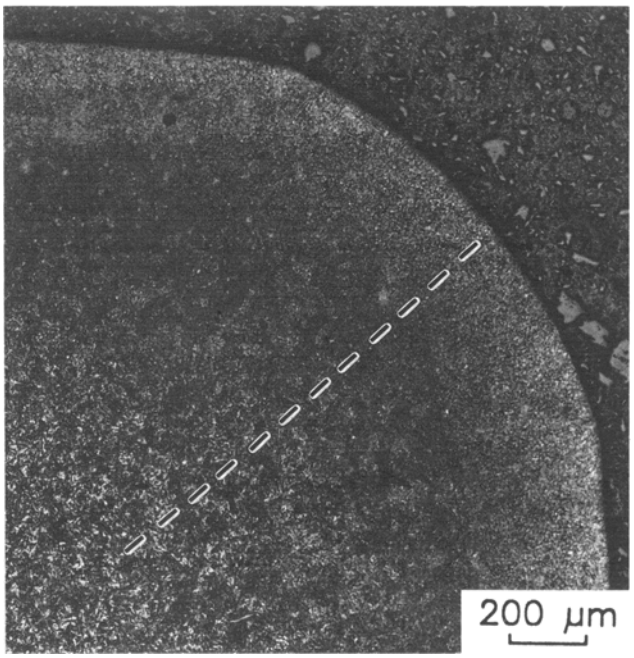

Fig. 6 Location of corner microhardness profiles.

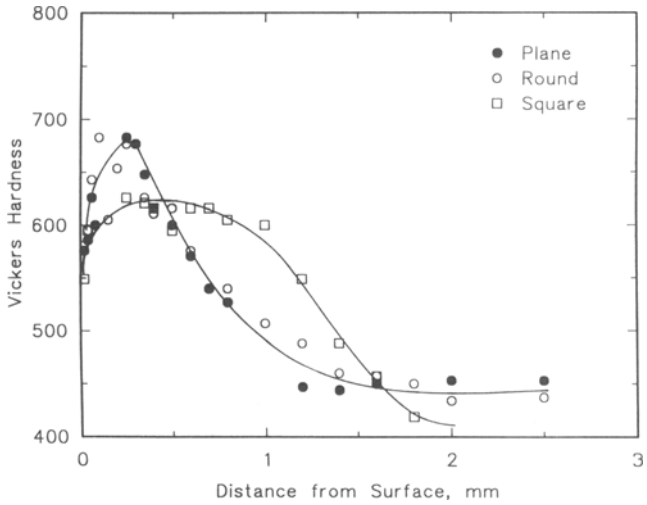

Fig. 7 Microhardness profiles from a square corner, a rounded corner, and a plane surface away from the corners.

4. Results

4.1. *Microstructure and Hardness*

Light micrographs illustrate the differences in microstructure between the square- and round-edged specimens. Figure 5 contains cross sections of each specimen geometry. At the relatively low magnification of Fig. 5(a) and (b), the case of tempered plate martensite appears grey and changes to the black and white appearance of the tempered lath martensite in the core. At a higher magnification, Fig. 5(c) and (d), the difference in corner microstructure is clearer. Martensite plates etch dark and the surrounding austenite appears white. There is more retained austenite near the square corner (Fig. 5c) than at the round corner (Fig. 5d). The maximum amount of retained austenite at the square corner was optically measured to be 33%. The retained austenite at the round corner and along the plane surfaces is about 23%.

The locations of hardness profiles are superimposed on light micrographs of the specimens in Fig. 6. The corner profiles were taken on a diagonal traverse, and plane-surface hardness profiles were taken perpendicular to the flat surfaces of the specimens. Figure 7 compares microhardness profiles of carburized specimens at a square corner with those of a round corner and a plane surface. The plane surfaces of the square- and round-edged specimens have almost identical hardness profiles. The hardness at a square edge, close to the surface, is lower than that at comparable plane and round edge locations. However, as the profile depth increases, the hardness at a square edge eventually exceeds that of the other specimen locations. The case depth of the round corner and of the plane surface is 1.0 mm (0.040 in.), whereas the square corner measured above 50 HRC as far as 1.4 mm (0.057 in.) along the diagonal. Both specimen geometries exhibit similar surface oxidation, with a maximum depth of 7 μm (0.00028 in.).

The core microstructures were similar for the two specimen geometries. Figures 8(a) and (b) show the tempered lath martensite of the cores for the round- and square-edged specimens, respectively. Figure 8(c) is a light micrograph of a cross section surface metallographically prepared to reveal austenite grain boundaries. The prior austenite grain size was measured to be ASTM 7.5 (27 μm).

The range of surface roughness measurements, R_a, for the specimens is 0.33 to 0.98 μm (13 to 39 μin.), with an average of 0.58 μm (23 μin.). Within this roughness range, there was no re-

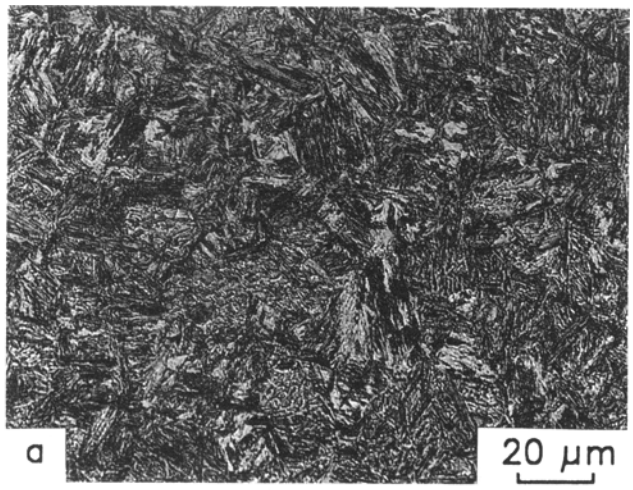

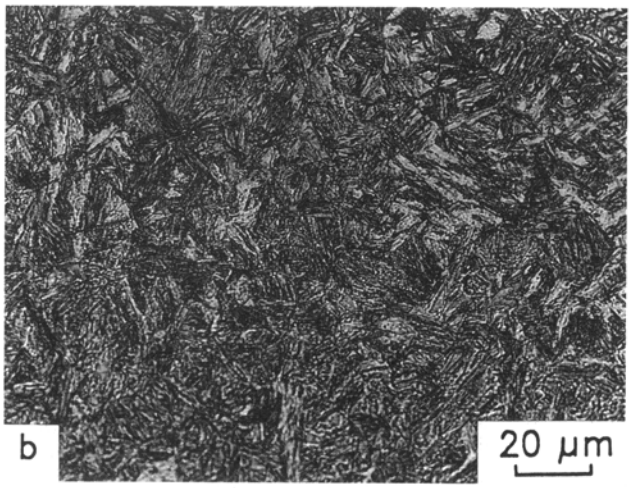

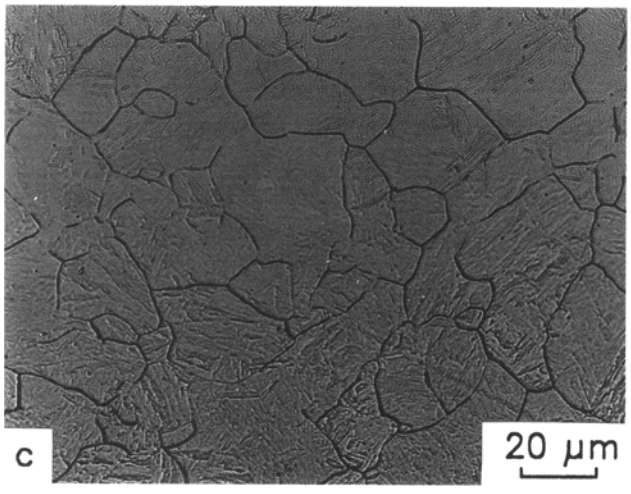

Fig. 8 Core microstructures. **(a)** Round-edged specimen. **(b)** Square-edged specimen. **(c)** Austenite grain boundaries. Light micrographs.

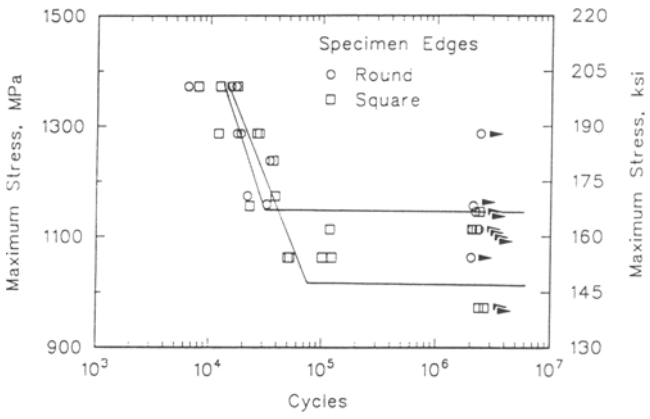

Fig. 9 *S-N* plot for SAE 4320 bending fatigue specimens of two geometries.

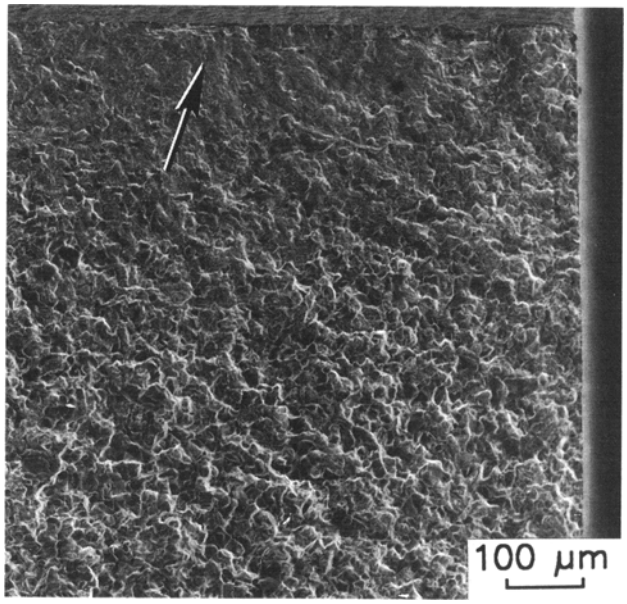

Fig. 10 SEM micrograph of fracture surface of a square-edged specimen. Arrow indicates an initiation site approximately 500 μm from the square corner.

lationship between the variation in average surface roughness and fatigue performance.

4.2. *Fatigue Performance*

The bending fatigue performance of square- and round-edged specimens is summarized in Fig. 9, a standard *S-N* diagram of stress versus cycles to failure. Both data sets exhibit standard *S-N* curves with well-defined endurance limits. At the higher stress levels, above about 1175 MPa (170 ksi), there is no difference in the fatigue behavior of the two geometries. However, the fatigue limit of the rounded specimens is higher,

1150 MPa (165 ksi), compared to approximately 1000 MPa (145 ksi) for the square-edged specimens. The endurance limits established in this study are slightly lower than that reported for SAE 4320 carburized steel by Erven, perhaps because of grain size differences.[4,5] The carburized specimens examined by Erven had a prior austenite grain size of ASTM 8.4 (20 μm), whereas the grain size of the specimens examined here is ASTM 7.5 (27 μm).

Fatigue crack initiation occurred in both geometries at the surface on the tension side of the specimens along the line of maximum stress at the base of the radius. The specimen geometry influenced where along the line of maximum stress the initiations occurred. For example, Fig. 10 is an SEM fractograph of a square-edged specimen with a fatigue crack that began about 500 μm from the corner. In the square-edged geometry, all of the specimens showed fatigue cracks associated with the square edge, usually about 200 to 900 μm from the corner. Only about 10% of the round-edged specimens had initiation sites within 1.0 mm of the specimen edge. The balance of the initiation sites in the round-edged specimens was randomly distributed along the central region of the line of maximum stress.

The majority of initiation sites was intergranular, but the initiation of fatigue cracks was occasionally associated with inclusions or surface defects. Figure 11 shows SEM fractographs of a typical fatigue crack in one of the square-edged SAE 4320 carburized steel specimens. Figure 11(a) shows two initiation sites indicated by arrows. The site marked b, about 300 μm from the corner, is shown in detail in Fig. 11(b). The small intergranular initiation is surrounded by a transgranular region of stable fatigue crack growth. The case fracture surface becomes predominantly intergranular once overload occurs. Figure 11(c) is a high-magnification fractograph of the intergranular initiation. This intergranular type of initiation is associated with phosphorus segregation and cementite formation on austenite grain boundaries.[18-20]

Most (73%) of the failed specimens, with both geometries, had multiple initiation sites. For example, Fig. 12(a) shows two sites where cracks initiated on different planes and formed a step or ratchet mark on the fracture surface. Multiple initiation sites and ratchet marks are common features of fatigue fractures resulting from relatively high nominal stress.[21] The specimen in Fig. 12(a) has square edges and failed at 1155 MPa (168 ksi) after 22,700 cycles. Figure 12(b) shows two initiation sites on the fracture surface of a round-edged specimen that failed after 17,400 cycles at 1285 MPa (185 ksi).

Multiple initiation sites develop even at applied stress levels just above the endurance limits for the two types of specimens, and the number of multiple sites tends to increase with increasing applied stress. Table 4 lists the total number of initiation sites for each specimen and the number of initiation sites within 1.0 mm of the edge of the specimen. High-magnification examination of all initiation sites showed most sites associated with intergranular crack initiation exemplified by Fig. 11. Other work has shown that intergranular cracks that become the sites for transgranular fatigue crack propagation in carburized steel are initiated by the first load application prior to cyclic loading.[22] In view of this mechanism of fatigue crack initiation, the results in Table 4 show that square-edged specimens are more sensitive to intergranular crack initiation than

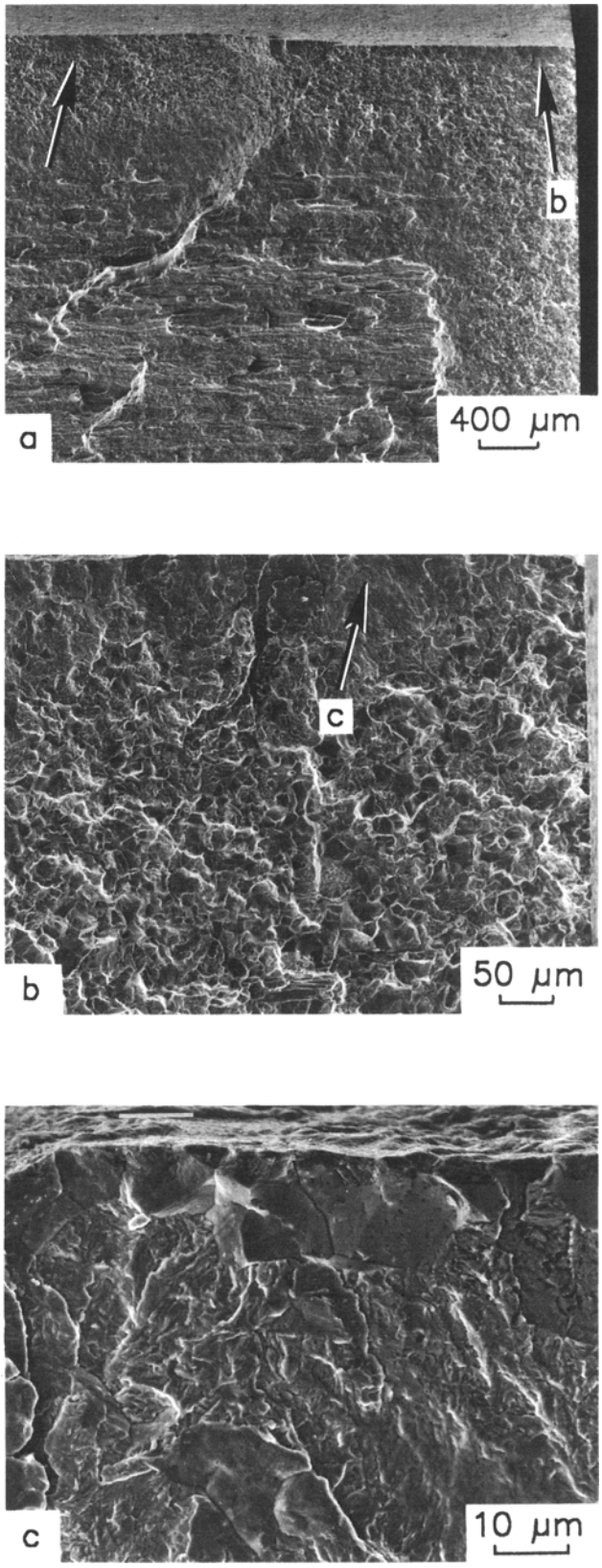

Fig. 11 SEM micrographs of typical bending fatigue fracture surface of carburized SAE 4320 steel. **(a)** Arrows indicate two initiation sites. **(b)** Higher magnification of site b showing the transgranular crack zone. **(c)** Intergranular initiation site.

Table 4 Initiation Sites in Bending Fatigue of Carburized Steel

Stress, MPa	Total sites	Corner sites(a)
Square-edged specimens		
1370	3	1
1370	4	1
1370	4	2
1285	1	1
1285	2	1
1285	1	1
1235	2	1
1175	1	1
1155	2	1
1115	1	1
1060	3	1
1060	2	1
1060	1	1
1060	3	1
Round-edged specimens		
1370	2	0
1370	2	0
1370	5	1
1285	2	0
1285	3	0
1235	2	0
1175	3	0
1160	1	0

(a) Initiation sites within 1.0 mm of specimen corner.

are round-edged specimens. Reasons for the specimen geometry influence on fatigue performance are discussed below.

5. Discussion

In cantilever beam fatigue testing of carburized steel, the loading conditions, residual stresses, and microstructure must be considered. The specimens are loaded such that the maximum tensile stress occurs at the surface of the specimen across the base of the radius, simulating the root of a gear tooth. The applied tensile stresses interact with the residual compressive stresses along the line of maximum stress at the base of the radius of both specimen geometries. The square-edged and round-edged specimens behave similarly in the low-cycle fatigue region, but square-edged specimens have a lower endurance limit than round-edged specimens. The endurance limits are 1150 MPa (165 ksi) and 1000 MPa (145 ksi) for the round- and square-edged specimens, respectively, a difference of 13%. This difference in fatigue performance is related to an increased sensitivity to intergranular cracking in the square-edged specimens at low stress levels. This increased sensitivity is, in turn, related to the increase in retained austenite noted at the corners of the square-edged specimens, a factor that is explained by reduced diffusion of carbon at square specimen edges.[2,3] At the edges, the different microstructures (Fig. 5) reflect the difference in residual stresses at the corners, i.e., less

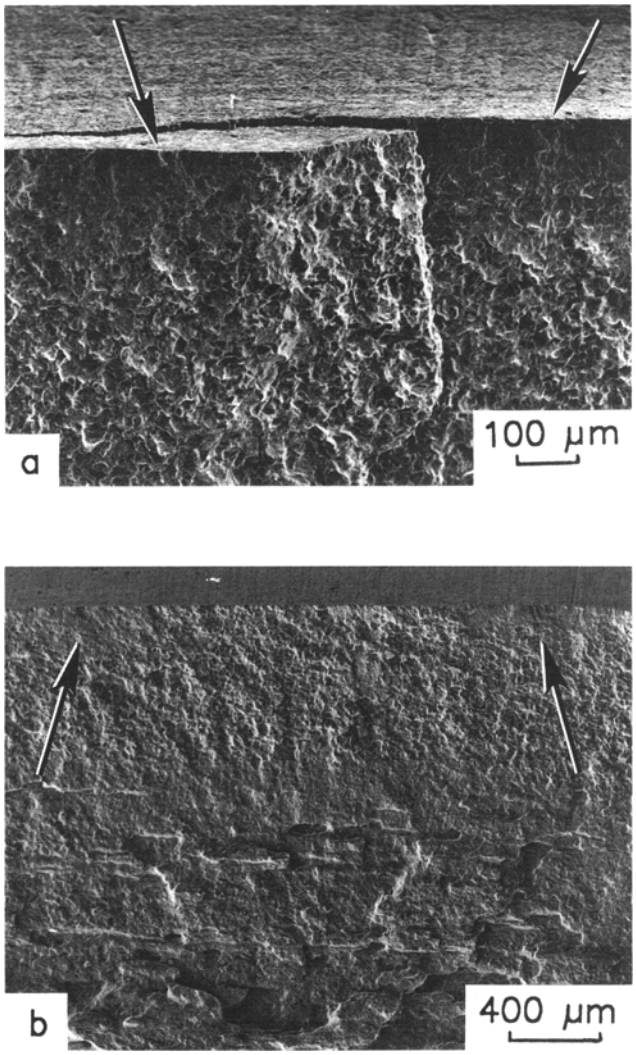

Fig. 12 SEM micrographs of multiple initiation sites in bending fatigue of carburized SAE 4320. **(a)** Square-edged specimen. **(b)** Round-edged specimen.

austenite transformation during quenching results in lower surface compressive stresses near the square specimen corners.

With lower compressive stresses along the line of maximum stress on the specimen surface near the square edge compared to the central area of the specimen, lower applied tensile stresses would be required to initiate intergranular cracking. Residual stress measurements confirmed that the surface compressive stresses are lower close to square specimen edges, 150 MPa (22 ksi), than at central locations, 180 MPa (26 ksi). The residual stress differences provide preferential initiation sites approximately 200 to 900 μm from the square edge along the line of maximum stress of the modified Brugger specimens.

The corner effect may be exaggerated at higher carburizing temperatures. The specimens tested by Jones and Krauss, carburized at the higher temperature of 1050 °C, had larger amounts of retained austenite, on the order of 55%.[2] The more severe corner microstructure produced at higher carburizing temperatures may result in even lower compressive residual

stresses and a more dramatic decrease in bending fatigue performance.

The results of this investigation have shown that specimen corner geometry, even in specimens carburized at conventionally low temperatures (930 °C), can affect fatigue performance. Therefore, although not a large factor, specimen geometry may have contributed to the scatter in fatigue endurance limits reported in the literature.[1] Even greater effects of corner geometry, as demonstrated by Jones and Krauss,[2,3] would be expected for specimens carburized at higher temperatures.

6. Conclusions

- Square edges of carburized fatigue specimens contain more retained austenite and have lower compressive residual stresses than specimens with rounded edges.
- At high applied stress levels, specimen geometry and the resultant microstructure have little influence on low-cycle fatigue behavior.
- Square-edged specimens have a lower fatigue limit due to an increase in sensitivity to intergranular crack initiation within about 1.0 mm of the square edge. For specimens gas carburized at 930 °C, the bending fatigue limits are on the order of 10% lower for square-edged specimens compared to round-edged specimens.

Acknowledgments

This project was part of the carburizing steel program of the Advanced Steel Processing and Products Research Center, an NSF Industry-University Cooperative Research Center in the Department of Metallurgical and Materials Engineering at the Colorado School of Mines. The authors thank Kirk Erven, The Timken Company, for his assistance with many of the testing techniques; The Timken Company, for providing the steel; Jon Dossett, Midland Metal Treating, for surface measurements and carburizing the specimens; and Butch Brewer, Colorado School of Mines, for metallography.

References

1. R.E. Cohen, P.J. Haagensen, D.K. Matlock, and G. Krauss, "Assessment of Bending Fatigue Limits for Carburized Steel," SAE Technical Paper Series No. 910140, 1991.
2. K.D. Jones and G. Krauss, "Effects of High-Carbon Corners on Microstructure and Fatigue of Partial Pressure Carburized Steel," in *Heat Treatment '79*, The Metals Society, London, 1979, p 188-193.
3. K.D. Jones and G. Krauss, "Microstructure and Fatigue of Partial Pressure Carburized SAE 8620 and EX 24 Steels," *J. Heat Treating*, Vol 1 (No. 1), 1979, p 64-71.
4. K.A. Erven, D.K. Matlock, and G. Krauss, "Effect of Sulfur on Bending Fatigue of Carburized Steel," *J. Heat Treating*, Vol 9, 1991, p 27-35.
5. J.L. Pacheco and G. Krauss, "Microstructure and High Bending Fatigue Strength in Carburized Steel," in *Carburizing: Processing and Performance*, G. Krauss, Ed., ASM International, 1989, p 191-237.
6. R. Sieber, "Bending Fatigue Performance of Carburized Gear Steels," SAE Technical Paper Series No. 920533, 1992.
7. H. Brugger and G. Kraus, "Influence of Ductility on the Behavior of Carburizing Steel During Static and Dynamic Bend Testing," *Archiv. Eisenhüttenwesen*, Vol 32, 1961, p 529-539.
8. T.B. Cameron and D.E. Diesburg, "The Significance of the Impact Fracture Strength of a Carburized Steel," in *Case-Hardened Steels: Microstructural and Residual Stress Effects*, D.E. Diesburg, Ed., The Metallurgical Society of AIME, 1984, p 17-32.
9. R.A. DePaul, "Impact Fatigue Resistance of Carburized Gear Steels—Development of a Testing Machine and Evaluation of Initial Test Results," *Mater. Res. Stand.*, Mar, 1970, p 15-17, 54, 56-57.
10. R.A. DePaul, "High Cycle and Impact Fatigue Behavior of Some Carburized Gear Steels," *Met. Eng. Quart.*, Nov, 1970, p 25-29.
11. J.J. deBarbadillo, "The Effect of Impact Fatigue Prestressing on the High Cycle Fatigue Resistance of Carburized Gear Steels," SAE Technical Paper Series No. 730142, 1973.
12. D.E. Diesburg and G.T. Eldis, "Fracture Resistance of Various Carburized Steels," *Metall. Trans. A*, Vol 9, Nov 1978, p 1561-1571.
13. K.A. Erven, "The Effects of Sulfur and Titanium on Bending Fatigue Performance of Carburized Steels," M.S. thesis No. T-3849, Colorado School of Mines, July 1990.
14. C.J. Van Tyne and K.A. Erven, "Finite Element Modelling of Carburizing Using a Commercial Code," in preparation. Presentation summarized in J.E. Morral and A.D. Romig, Jr., "Computer Programs for Modeling Diffusion-Controlled Processes," JOM, Feb 1992, p 12-14.
15. R.E. Peterson, *Stress Concentration Factors*, John Wiley & Sons, 1974, p 98.
16. *Residual Stress Measurements by X-Ray Diffraction*, SAE J784a, 2nd ed., 1971.
17. A.W. Brewer, K.A. Erven, and G. Krauss, "Etching and Image Analysis of Prior Austenite Grain Boundaries in Hardened Steels," *Materials Characterization*, Vol 27, 1991, p 53-56.
18. G. Krauss, "The Microstructure and Fracture of a Carburized Steel," *Metall. Trans. A*, Vol 9, 1978, p 1527-1535.
19. H.K. Obermeyer and G. Krauss, "Toughness and Intergranular Fracture of a Simulated Carburized Case in EX-24 Type Steel," *J. Heat Treating*, Vol 1 (No. 3), 1980, p 31-39.
20. T. Ando and G. Krauss, "The Effect of Phosphorus Content on Grain Boundary Cementite Formation in AISI 52100 Steel," *Metall. Trans. A*, Vol 12, 1981, p 1283-1290.
21. D.J. Wulpi, *How Components Fail*, American Society for Metals, 1966.
22. R.S. Hyde, R.E. Cohen, D.K. Matlock, and G. Krauss, "Bending Fatigue Crack Characterization and Fracture Toughness of Gas Carburized SAE 4320 Steel," SAE Technical Paper Series No. 920534, 1992.